Influence of Atmospheric Stability on the Size Distribution of the Vertical Dust Flux Measured in Eroding Conditions Over a Flat Bare Sandy Field

Bouthaina Khalfallah, C Bouet, M.T. T Labiadh, S.C. C Alfaro, G. Bergametti, B. Marticorena, S. Lafon, S. Chevaillier, A. Féron, P. Hease, et al.

Influence of atmospheric stability on the size-distribution of the vertical dust flux measured in eroding conditions over a flat bare sandy field

B. Khalfallah[1], C. Bouet[1,2], M. T. Labiadh[3], S. C. Alfaro[1], G. Bergametti[1], B. Marticorena[1], S. Lafon[1], S. Chevaillier[1], A. Féron[1], P. Hease[1], T. Henry des Tureaux[2], S. Sekrafi[3], P. Zapf[1], and J. L. Rajot[1,2,3]

[1]LISA (Laboratoire Interuniversitaire des Systèmes Atmosphériques), UMR CNRS 7583, Université Paris Est Créteil - Université de Paris, Institut Pierre Simon Laplace, F-94010 Créteil, France.

[2]iEES Paris (Institut d'Ecologie et des Sciences de l'Environnement de Paris), UMR IRD 242, Université Paris Est Créteil - Sorbonne Université - CNRS - INRA - Université de Paris, F-93143 Bondy, France.

[3]IRA (Institut des Régions Arides) de Médenine, El Fjé, 4119, Tunisia.

Corresponding author: Bouthaina Khalfallah (Bouthaina.Khalfallah@lisa.u-pec.fr)

Key Points:

- The size-resolved dust flux was measured during eight erosion events by the gradient method
- The size-distribution of the dust flux depends on the surface layer stability conditions
- The vertical dust flux is enriched in submicron particles in thermally unstable conditions

Abstract

In spite of their importance for the modeling of the atmospheric cycle of mineral dust, measurements of the intensity and size-distribution of the dust emission flux produced by wind erosion in natural conditions remain rare. During the WIND-O-V's (WIND erOsion in presence of sparse Vegetation) 2017 experiment, 8 major erosion events having occurred on a sandy flat field of southern Tunisia were documented. Consistent with the small size (90 µm) of the erodible sand grains and the low aerodynamic roughness length (Z_0 < 0.079 cm), the threshold for wind erosion was low (u_{*t} = 22 cm s^{-1}). The classical gradient method was applied to assess the size-resolved vertical dust flux, and the stability of the atmosphere quantified by the means of the Richardson number (Ri) as well as of its shear stress (u_*) and thermal gradient ($\partial\theta/\partial z$) components. The vertical dust flux increased with u_* following a power law but the number size-distribution of the dust flux was found to be significantly richer in submicron particles in thermally unstable than in stable periods. This challenges the usual assumption that, independently of their size, the particles smaller than 10 µm follow equally the movements of the air masses in which they are embedded and that the thermal stratification of the surface layer does not affect the size-distribution of the surface flux when measured a few meters above the ground. Finally, we propose a simple empirical method for taking this influence of the thermal instability into account.

1 Introduction

When the stress exerted by the wind becomes large enough, loose particles present on the surface of arid and semi-arid soils are set into motion. Within approximately the first meter above the surface, the size of these wind-eroded particles ranges from a fraction of micrometer to a few millimeters. However, only the particles with a diameter smaller than 20 µm (PM_{20}) (Gillette, 1981; Shao, 2008) have a residence time in the troposphere long enough to be transported hundreds or thousands kilometers away from their source (e.g., Prospero, 1999; Schütz, 1980). According to current estimates (e.g., Boucher et al., 2013), between 1000 to 4000 Tg of mineral particles are thus injected yearly into the atmosphere.

As compared to the composition of the surface horizon of the parent soils, PM_{20} are enriched in soil nutrients and their export has negative effects on the fertility of agricultural soils (e.g., Sterk et al., 1996; Webb et al., 2012). Conversely, at the other end of their atmospheric cycle, deposition of eroded particles can constitute a precious source of nutrients for depleted continental (Okin et al., 2004; Swap et al., 1992) or marine (e.g. Duce et al., 1991; Jickells et al., 2005) areas. During their stay in the atmosphere, particles impact the Earth's climate directly by scattering and absorbing solar and terrestrial radiations (e.g., Sokolik et al., 2001; Sokolik & Toon, 1996), but they can also affect it indirectly by favoring the formation of clouds (e.g., DeMott et al., 2003; Sassen et al., 2003) or modifying their micro-physical properties (e.g., Min et al., 2009; Weinzierl et al., 2017). Finally, airborne mineral dust was identified to impact negatively human health worldwide (e.g., Hashizume et al., 2010; de Longueville et al., 2013; Morman & Plumlee, 2013).

Several physical schemes have been developed to predict the characteristics of the PM_{20} emission flux as a function of both the wind shear stress and the state of the soil surface. Basically, two mechanisms are generally considered as being responsible for the emission of these particles: 1) direct aerodynamic entrainment (e.g., Klose & Shao, 2013), and 2) the combination of saltation and sandblasting.

In most arid and sparsely vegetated semi-arid soils, the amount of sand-sized grains easily set into motion by the wind is not a limiting factor and the second mechanism is assumed to be predominant (Shao et al., 2011). For wind friction velocities above the threshold of motion, the heavy sand grains start moving in approximately the first meter above the surface (saltation process) and a fraction of their kinetic energy is used for releasing the finer PM_{20} particles (sandblasting process). Thus, saltation appears as a necessary prerequisite for the emission of the PM_{20}, which is in good agreement with most observations performed either in laboratory wind-tunnels (Alfaro et al., 1997, 1998; Shao et al., 1993) or in outdoor conditions on naturally eroding fields (Gillette, 1977; Gillette et al., 1997; Gillette & Walker, 1977; Gomes et al., 1990; Ishizuka et al., 2014; Sow et al., 2009). Because of the large size of the grains entering saltation, this process is the easiest to observe and in the wake of the pioneering work of Bagnold (1941) an abundant literature has been dedicated first to its parametrization (see the review of Greeley & Iversen (1985)) then to its physical modeling (e.g., Marticorena & Bergametti, 1995; Owen, 1964; Shao & Li, 1999). Much fewer theories, in fact only three, have been proposed for explaining the emission of PM_{20} in presence of saltating sand grains and predicting their size-distribution. Based on wind-tunnel observations, Alfaro & Gomes (2001) considered that the PM_{20} preexisted in the saltating aggregates or in the soil and that a fraction of the kinetic energy of the saltators was used to counterbalance the binding energies of these fine particles and eventually release them. Shao (2001) also considered that the impact of the saltators on the soil lead to its partial disaggregation. In spite of their differences, the two models agreed on the fact that the size-distribution of the ejected particles should depend on the energy of the saltators, and therefore on wind speed. This point was challenged by Kok (2011a) who proposed the 'brittle' theory in which it was considered that the PM_{20} size-distribution did not depend on the speed of the wind (Kok, 2011b). Whatever the exact nature of the process, dust particles are released once the kinetic energy of saltating particles exceeds their binding energy. Then, turbulent diffusion contributes to their transport towards higher levels thus opposing the effect of gravity that tends to maintain them close to the surface.

Thus, the vertical flux (F_v) in the Surface atmospheric Boundary Layer (SBL) is the sum of the upward diffusive flux and the downward settling one and is often referred to as the 'net' flux. It is found to increase with the wind stress following a power law similar to that proposed by Gillette & Passi (1988):

$$F_v = C(u_*)^n(1 - \frac{u_{*t}}{u_*}) \quad (1)$$

In this equation, u_* is the wind friction velocity, u_{*t} the threshold wind friction velocity above which saltation occurs, and C and n are constants. In their original work, Gillette & Passi (1988) suggested that the exponent n should be equal to 4 but field measurements indicate that it is actually more variable (e.g., Ishizuka et al., 2014).

Two methods exist for measuring F_v. One aims at applying the eddy covariance method to the determination of the size-resolved vertical dust flux (Fratini et al., 2007; Porch & Gillette, 1977). Though promising, its application to dust particles remains complicated because of the current lack of instruments being at the same time able to acquire at high frequency the fluctuations of the very low number concentrations of the coarsest dust particles and small enough not to disturb the micrometeorological measurements performed in parallel at the same point. The second method, usually referred to as the 'gradient method', was designed by Gillette et al. (1972). In the framework of the AMMA (African Monsoon Multidisciplinary Analysis; Redelsperger et al., 2006) international campaign, this method was improved by the use of an Optical Particle Counter (OPC) to document the effect of u_* on the size-resolved dust emission flux over a bare agricultural field in Niger (Sow et al., 2009). The method was also used for the same purpose during the Japan-Australia Dust Experiment (JADE; Ishizuka et al., 2014). This method is well adapted to the measurement of the dust flux size distribution up to diameters of approximately 20 µm (Gillette et al., 1972).

Basically, the 'gradient method' is an adaptation of the K-theory, which considers that, in the constant flux layer above the ground, the vertical turbulent flux of a scalar is simply proportional to the vertical gradient of its mean concentration. When applied to dust, this gives:

$$F_v = -K_p \frac{dC}{dz} \quad (2)$$

with K_p the turbulent eddy diffusivity of the dust particles and C the dust concentration (in particles m^{-3} or kg m^{-3}).

Then, assuming neutral conditions and that the vertical transport of particles with a diameter ≤ 20 µm is similar to that of momentum, Gillette et al. (1972) obtained:

$$F_v = u_* k \frac{C_l - C_h}{\ln\left(\frac{z_h}{z_l}\right)} \quad (3a)$$

where k is the von Karman's constant (k = 0.4), and C_l and C_h are the dust concentrations measured in the SBL at a low (z_l) and high (z_h) heights (in m).

Because conditions are rarely neutral in natural conditions, Equation (3a) can be corrected using the stability function ψ_m (Businger et al., 1971) calculated using the Monin-Obukhov length (L):

$$F_v = u_* k \frac{C_l - C_h}{\ln\left(\frac{z_h}{z_l}\right) - \psi_m\left(\frac{z_h}{L}\right) + \psi_m\left(\frac{z_l}{L}\right)} \quad (3b)$$

Again, this correction assumes that the vertical transport of particles and momentum are similar. However, relatively ancient (Businger, 1986; Businger et al., 1971) and more recent (Abbasi et al., 2017; Li & Bou-Zeid, 2011; Smedman et al., 2007) studies indicate that even in slightly unstable conditions the ratio of the eddy diffusivity of scalars (water vapor, heat) to that of momentum increases dramatically, which means that these scalars are transported more efficiently than momentum. For particles, experimental data are missing but Freire et al. (2016) used Large Eddy Simulation (LES) to show that even in idealized conditions (spatially and temporally constant emission flux) atmospheric stability and particle size (in the range 1-30 µm) should be taken into account in the derivation of the surface net flux from the vertical profiles of concentration measured in the surface boundary layer. Indeed, the simulations indicate that as for other scalars the vertical uptake of the finest particles by turbulence should be favored and this particularly in unstable conditions.

Therefore, we hypothesize that atmospheric instability could also play an important role in the more variable 'real life' conditions and have a quantifiable effect on the 1) magnitude and 2) size-distribution of the vertical dust flux in the surface layer. In order to validate or infirm these assumptions, we will use the results of the measurements performed in the frame of the

WIND-O-V's (WIND erOsion in presence of sparse Vegetation) 2017 experiment conducted over a flat bare field of southern Tunisia. The description of the experimental site and the details of the instrumentation and methods are given in the following 'Materials and methods' section; then the impact of atmospheric stability on the magnitude and size-distribution of the vertical flux is analyzed.

2 Materials and Methods

2.1 Site description

The experiment was carried out from 1 March 2017 to 15 May 2017 in the Dar Dhaoui experimental range (latitude 33°17′45″N, longitude 10°46′57″E) of the Institut des Régions Arides (IRA) of Médenine (Tunisia). The site, described in more details in Dupont et al. (2018, 2019), is located in the arid region of the Jeffara Plain. The parent soil is aeolian fine sand deposit generally lying on calcrete (Labiadh et al., 2013). Six composite samples, made of about 15 individual samples of loose soil surface particles (about 1 cm depth) were collected each ten meters along radii of the plot, and their size-distributions analyzed. Practically, this was done in two ways. On the one hand, composite soil samples were dry sieved following the methodology established by Chatenet et al. (1996). On the other hand, the soil organic matter was removed using H_2O_2 (H_2O_2 15% 24 h at 50°C and 72 h at 25°C), the samples were carefully rinsed with demineralized water, disaggregated for 1 minute with ultrasonic agitation and sodium hexametaphosphate added in order to maintain finer particles in suspension. A laser sizer (LS 230 Laser Diffraction Particle Size Analyser - Beckman Coulter©) was used to measure the totally dispersed soil distribution. In both cases, the median of the size distribution is 90 µm (Fig. 1). The mean mass of the soil fraction lower than 10 µm (corresponding approximately to the PM_{10} studied in the paper) represents 3.25% (Standard Deviation = 0.49%) of the soil sample (Fig. 1b). In order to meet the conditions of an ideal flat bare soil without soil crust or ridges, the surface was tilled with a disc plough and levelled with a wood board before the beginning of the experiment. During the experiment, the soil surface tended to evolve either because of a relative increase of its rough elements, of some rain events, or because of the beginning of vegetation growth. Thus, to maintain the ideal conditions we were seeking the surface was levelled again on 13-14 March and 19 April, and tilled and levelled on 29 April-1 May. The measurements were performed at the center of the southern limit of the experimental plot approximating a flat half-circle of 150 m radius (Fig. 2a). In the North, the fetch was slightly longer (about 200 m). The plot was surrounded by small bushes in the North-West (0.34±0.08 m height and 0.58±0.20 m diameter) and young olive trees arranged in a square pattern (about 1.7±0.3 m height, 1.5±0.4 m diameter, and 26 m spaced) in the North-East. The interested reader will find in supplementary material the study showing that, in spite of the relatively short fetch, the instruments located at the 4 m height are still in the constant flux layer, which ensures the applicability of the gradient method.

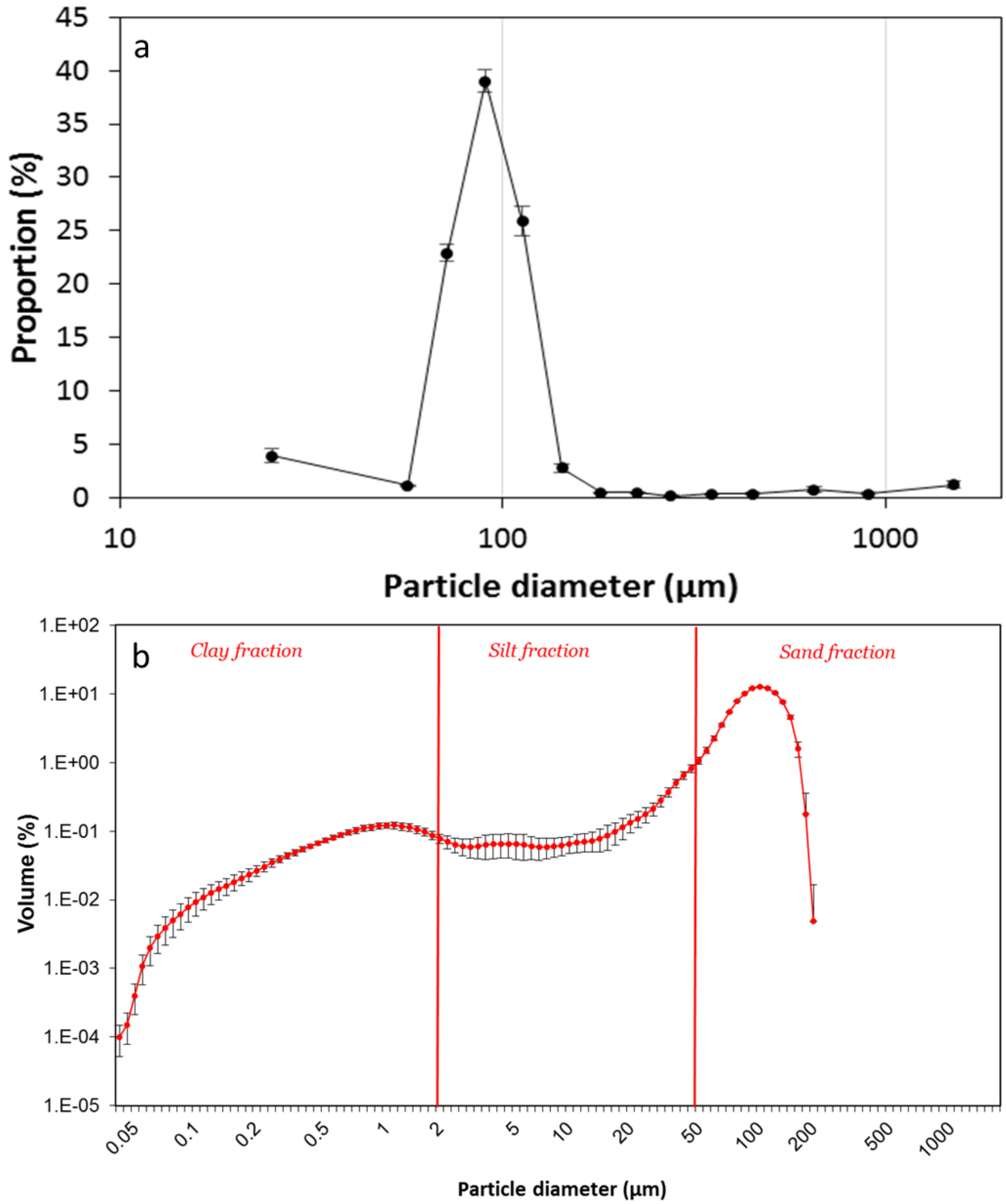

Figure 1. (a) Mean size distribution of the dry sieved soil. (b) Mean size distribution of the totally dispersed soil. Error bars represent the standard deviation of the mean of 6 composite soil samples.

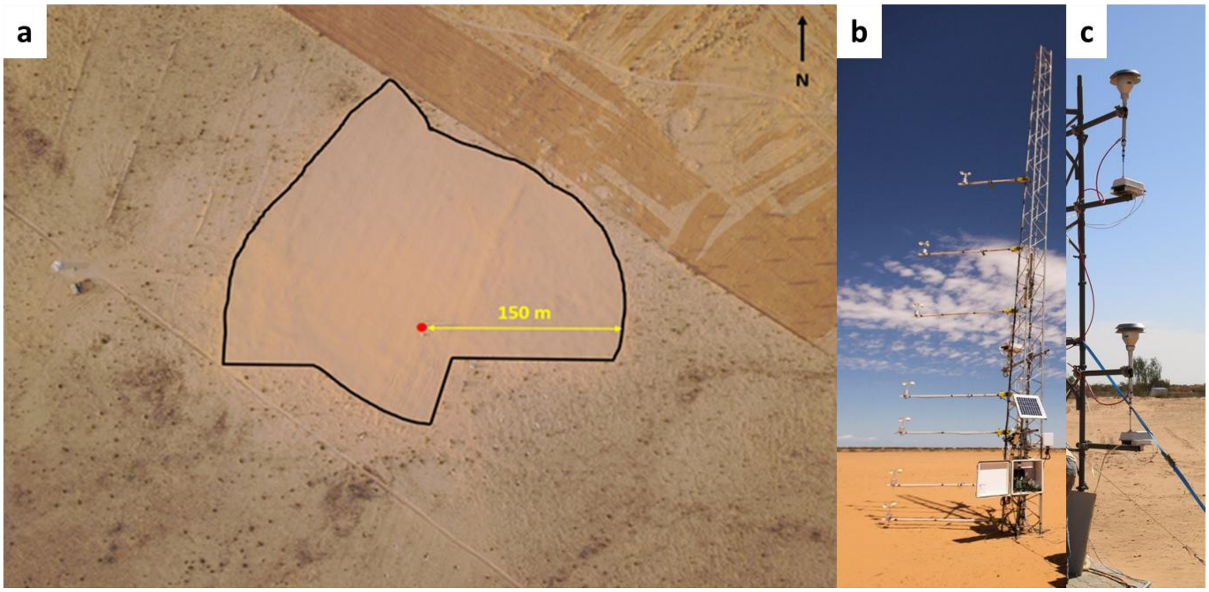

Figure 2. (a) Aerial view of the experimental plot (©IRD – IRA – Christian Lamontagne). The red dot indicates the location of the instruments; (b) View of the meteorological mast with the 7 cup anemometers; (c) View of the two OPCs with their TSP sampling heads.

2.2 Measurements

The calculation of the vertical dust flux based upon the gradient method requires to measure (1) the dynamical parameters characterizing the structure of the SBL (the wind friction velocity, u_*, surface roughness length, Z_0, and Monin-Obukhov's length, L) and (2) the dust concentrations at two heights (Eq. 3). The required instrumentation deployed during the WIND-O-V's 2017 experiment is described in this paragraph.

2.2.1 Meteorological parameters

A meteorological mast (Fig. 2b) was equipped with 7 cup anemometers (A100R Vector Instrument®; resolution = 0.25 m s^{-1}) positioned at 0.22, 0.65, 1.33, 1.83, 3.01, 4.00, and 5.24 m above ground level (agl), and 4 thermocouples (type T cupper/Constantan; resolution = 0.2°C) positioned at 0.48, 1.66, 3.83, and 5.07 m agl to measure simultaneously at 0.1 Hz the wind speed and air temperature vertical profiles, respectively. These meteorological measurements allowed the computation of the aerodynamic parameters necessary to apply the gradient method (u_*, Z_0, and L) as well as other quantities such as the Richardson number allowing to characterize the SBL stability.

Before being installed in the gradient position, anemometers were intercompared to test the consistency of their response in natural conditions. In all, 2542 data (5-min averages) were acquired in parallel by the 7 anemometers and their correlation to the mean measurements was excellent (R^2>0.99, with a slope ranging from 0.99 to 1.02).

Wind direction was derived from the measurements performed with a 3D sonic anemometer. Relative humidity was measured using an HMP60 probe (Campbell® Scientific Instruments).

2.2.2 Dust number concentrations

To measure the size resolved dust concentration, we used two OPCs (welas®, White Light Spectrometer 2300, PALAS) positioned at 2.04 and 4.10 m agl (Fig. 2c). These instruments are spectrometers deriving the air-suspended particles number concentration in predefined size classes from the light they scatter at 90° when illuminated by a white light source. The suction is done at a controlled flowrate of 5 L min^{-1} and each OPC was equipped with an omnidirectional Total Suspended Particles (TSP) sampling head (BGI by Mesa Labs, Butler, NJ USA). Vanderpool et al. (2018) conducted wind tunnel tests of six commonly used omnidirectional, low-volume inlets to determine their actual size-selective performance under conditions of expected use using solid, polydisperse aerosols at wind speeds of 2, 8, and 24 km/h (i.e., 0.56, 2.2, and 6.7 m s^{-1}, respectively). For the TSP inlet, the estimated total mass concentration collection efficiency was shown to increase with wind speed. For the coarsest particle size distribution (mass median diameter of 15 µm with a proportion of 93%), the estimated total mass concentration collection efficiency varied from 79% at 0.56 m s^{-1} to 99% at 2.2 m s^{-1}, and 102% at 6.7 m s^{-1}. Considering the range of wind velocity measured during the emission periods (> 5 m s^{-1} at about 2 m), we can expect that the use of the TSP inlet will not induce any significant loss of the coarse dust particles. The nominal flowrate of the TSP inlet is 16.7 L min^{-1}. So this flow was isokinetically split in two: a main flow immediately directed to the OPC through a short vertical tube to minimize the particle loss before measurement, and an auxiliary flow (11.7 L min^{-1}) controlled by an automated volumetric flow controller (MCR-50SLPM, Alicat Scientific). The time resolution of the measurements was 1 min.

The calibration was done by the company. The OPC calibration parameters were adjusted at the beginning of the experiment by following the routine calibration described in the welas® operating manual using the monodisperse caldust 1500 composed of silicon dioxide with a refractive index of $m = 1.43 - 0i$ in the visible wavelengths and a diameter of 1.28 µm so that the measured particle diameters correspond to optical diameters of spherical particles having an extinction efficiency equivalent to that of silica. We checked at the end of the experiment that the calibration parameters had not changed for the 2 OPCs. The particles are sorted into 15 diameter bins of equal logarithmic width (dlog(D)=0.125) ranging from 0.237 to 17.78 µm and centered on the mean geometric diameters (noted $D_{g,i}$ in the following) reported in Table S1 of the supplementary material. As recommended by the manufacturer, the number of particles counted in the smallest size class ($D_{g,1}$ = 0.27 µm) was considered as unreliable and thus discarded.

At the beginning and at the end of the campaign, the two OPCs were set up at the same level, 4.10 meters agl and along a west/east axis, to test the similarity of their response. The measured concentrations were found to be sufficiently large to allow a relevant inter-comparison only during the second period, which lasted from 10/05/2017 to 18/05/2017. For this comparison, data collected when wind directions were in the 80-100° and 260-280° sectors were rejected to avoid one OPC being shadowed by the other. When relative humidity was greater than 80%, particle concentration measurements were also rejected to avoid the risk of performing the inter-comparison in presence of fog droplets to which the instruments are also sensitive but not calibrated for. The correlation coefficients between the measurements of the two OPCs (16-min. average concentrations) are presented in Table S1 in supplementary material. It was > 0.9 (for n = 160) in all size-classes but the two coarsest in which the number concentrations were quite low ($D_{g,14}$ = 11.55 µm and $D_{g,15}$ = 15.40 µm, for which R^2 were 0.87 and 0.74, respectively). Therefore, these 2 size classes were discarded. The strong correlation existing in the remaining size-classes allows correcting easily one instrument according to the other. In order to avoid attributing more weight to the measurements performed by any which one of the two OPCs, they were successively chosen as the reference and the final concentration was determined as the arithmetical average of the two corrected concentrations.

In order to locate temporally the erosion events, we needed to be able to determine when the concentration at the lower level was significantly larger than that measured at the higher level. For this, we used the scatter around the mean of the difference of concentrations measured by the two instruments positioned at the same height and found that this threshold corresponded to be a relative difference of 23% in the 1.15 µm size class.

2.3 Dust flux computation

The wind friction velocity (u_*), surface roughness length (Z_0), and Monin-Obukhov's length (L) can be determined using the measured wind speed and temperature profiles according to the Monin-Obukhov theory (Monin & Obukhov, 1954):

$$U(z) = \frac{u^*}{k}\left[ln\left(\frac{z}{Z_0}\right) - \psi_m\left(\frac{z}{L}\right) + \psi_m\left(\frac{Z_0}{L}\right)\right] \tag{4}$$

$$\Delta\theta = \theta(z_h) - \theta(z_l) = \frac{\theta^*}{k}\left[ln\left(\frac{z}{Z_0}\right) - \psi_h\left(\frac{z}{L}\right) + \psi_h\left(\frac{Z_0}{L}\right)\right] \tag{5}$$

where θ^* is the characteristic dynamical temperature (in K), and $\theta(z_l)$ and $\theta(z_h)$ the temperature (in K) at measurement heights z_l and z_h (in m), respectively, and ψ_h the heat stability function.

In this study, u_*, Z_0, and L were obtained using the iterative procedure optimized by Frangi & Richard (2000) for fitting the wind speed and temperature measurements to Eqs. (4) and (5), with the stability functions ψ_m and ψ_h respectively defined as:

- for $z/L < 0$ (unstable cases; Dyer & Hicks, 1970; Hicks, 1976; Paulson, 1970):

$$\psi_m\left(\frac{z}{L}\right) = 2\,ln\left(\frac{1+x}{2}\right) + ln\left(\frac{1+x^2}{2}\right) - 2\arctan(x) + \frac{\pi}{2} \tag{6}$$

$$\psi_h\left(\frac{z}{L}\right) = 2\,ln\left(\frac{1+y}{2}\right) \tag{7}$$

With (Dyer, 1974):

$$x = \left[1 - 15\frac{z}{L}\right]^{1/4} \text{ and } y = \left[1 - 15\frac{z}{L}\right]^{1/2} \tag{8}$$

- for $z/L > 0$ (stable cases; (Webb, 1970):

$$\psi_m = \psi_h = -5\frac{z}{L} \tag{9}$$

Noteworthy, the gradient method used for the inversion of the dynamical parameters assumes the use of at least 10-min wind speed averages so that the major time scales of turbulence occurring in the SBL are integrated (Wieringa, 1993). In this study, we used 16-min averages for wind speed and air temperature following the results obtained by Dupont et al. (2018) on the same field.

The quality of the inversion of the dynamical parameters was carefully examined by using criteria similar to those defined by Marticorena et al., 2006):

1. Computation of the dynamical parameters were only done for directions where the experimental device could not perturb the measurements, i.e. between [265°, 360°] and [0°, 95°] (Fig. 2a).
2. Although the minimal wind speed that anemometers can measure is 0.25 m s^{-1}, we considered that a minimum wind speed of 1 m s^{-1} was required to have a sufficient precision to obtain a correct wind profile. Thus, the computation of the aerodynamic parameters were performed only when all the anemometers measured a wind speed greater than 1 m s^{-1}.
3. The quality of the inversion procedure was considered acceptable only if the difference between the computed and measured profiles was less than 5% for wind speeds and less than 0.2 K for temperatures.
4. To eliminate the possible cases of free convection, the profiles for which the fitted wind friction velocity u_* was lower than 0.2 m s^{-1} were also rejected.

In the “gradient configuration”, a dust emission event is defined as a period during which 1) the concentration of the lowest OPC in one of the most abundant size-classes (1.15 µm) is greater than 5 particle cm^{-3} and 2) the relative difference ($(C_l–C_h)/C_l$) between the bottom and upper concentrations is positive and larger than the threshold defined from the intercomparison of the two OPCs. For the same reason as during the OPC intercomparison, particle concentration measurements were also rejected when relative humidity was greater than 80%. The vertical dust flux was calculated only when all these conditions were fulfilled.

The total number flux, $F_{v,n}$, over the size range 0.32-10.00 µm in diameter is thus obtained by summing the dust fluxes calculated in each of the twelve retained individual size classes:

$$F_{v,n} = \sum_{i=2}^{13} \left(\frac{dF_{v,i}}{dLog(D_{g,i})}\right) dlog(D_{g,i}) \tag{10}$$

The derivation of the total mass flux, $F_{v,m}$, from the total number flux, $F_{v,n}$, was done (i) assuming spherical particles and (ii) using the equivalent mass density measured by Sow et al. (2009) during dust emission events in Niger ($\rho_d = 2.38 \pm 0.24$ g cm^{-3}). The hypothesis of particle sphericity is generally adopted even though several studies suggest that the aspect ratio for African dust particles is probably close to 1.5-1.7 (e.g., Chou et al., 2008; Kandler et al., 2007; Klaver et al., 2011). The equivalent mass density we used is slightly lower than the density of pure quartz (2.65 g cm^{-3}) generally adopted for dust particles in modelling studies but the value of 2.38 g cm^{-3} appears reasonable because African dust particles are known to be complex clusters of various minerals, mainly clays, calcite, quartz, feldspars and iron oxides (e.g., Kandler et al., 2009; Nowak et al., 2018) with voids in-between.

Noteworthy, the flux yielded by the gradient method (Equation 3b) is actually the net vertical flux (positive upward), which is to say the sum of the diffusive (F_d) and the negative gravitational settling (F_s) fluxes.

$$F_v = F_d + F_s \tag{11}$$

In the gradient theory, F_d is the flux assumed to be constant from the surface to the top of the surface boundary layer. Therefore, F_d is supposed to represent the flux of particles released from the surface before it is modified by upward transport and sedimentation.

F_s, which is simply the product of the gravitational settling velocity (given by the Stokes formula) and concentration for a given particle size, also depends on the altitude. Therefore, F_v is also elevation-dependent in the SBL and should be corrected to compensate the effect of gravitation (Shao, 2008) to retrieve F_d. However, in their exploitation of the JADE campaign, Shao et al. (2011) showed that this size-dependent correction is relatively limited as it was less than 2% for particles smaller than 3 µm and did not exceed 15% for particles with sizes up to 8.4 µm for $\Delta z \sim 2$ m. We also computed the correction for all size classes and found it to be less than 1% for particles smaller than 3.5 µm and less than 4% for particles with sizes ranging from 4 µm to 8.5 µm. Though small, this correction was applied to all the vertical dust fluxes we computed.

2.4 Atmospheric stability

Atmospheric stability is a result of the combination of thermal and dynamical effects: in a convective (unstable) boundary layer, turbulence is generated by buoyancy; in stable boundary layer, turbulence is suppressed by buoyancy while in neutral boundary layer, turbulence is generated by wind shear (Stull, 1988). Several parameters (see for instance Golder, 1972) can be used to quantify the stability of the atmosphere: the Monin-Obukhov length, the Richardson number, the bulk Richardson number, the Pasquill and Turner categories…. In this study, we selected the Richardson number, Ri (Richardson, 1920), which compares directly the atmospheric thermal source of instability to the dynamical one:

$$Ri = \frac{g}{T}\frac{\partial\theta/\partial z}{(\partial u/\partial z)^2} \tag{12}$$

where g is the acceleration of gravity (in m s^{-2}), T the absolute air temperature (in K), θ the potential temperature (in K), and u the mean wind speed (in m s^{-1}).

The sign of $\partial\theta/\partial z$ (equivalently that of Ri) indicates whether the atmosphere is thermally stable ($Ri > 0$) or unstable ($Ri < 0$), and the magnitude of Ri gives information on the predominance of dynamical vs. thermal effects on atmospheric stability. Note that at the very low altitude above sea-level of our experimental site (50 m), the potential (θ) and absolute (T) air temperatures can be approximated to be equal.

Practically, we have computed Ri using the equations proposed by Arya (1988) who expressed it as a function of the Monin-Obukhov length, L:

For $Ri < 0$:

$$\frac{Z_m}{L} = Ri(Z_m) \tag{13}$$

For $0 \leq Ri < 0.2$:

$$\frac{Z_m}{L} = \frac{Ri(Z_m)}{1-5Ri(Z_m)} \tag{14}$$

with Z_m (=1.56 m) the geometric mean of the minimum (Z_{min} =0.48 m) and maximum (Z_{max} =5.07 m) heights of the air temperature measurements.

3 Results

3.1 The dust emission events

The two OPCs were set in the gradient position from 5 March to 9 May 2017, and 8 periods were found to correspond to dust emission events identified according to the previously defined criteria (Tab. 1). Their durations vary from approximately 5 to 6 hours for Events 2, 5 and 6 to more than 9 hours for Events 4, 7 and 8. During the majority of these events, the wind blew rather constantly either from NNW (Events 1, 2, 3, and 5) or from NE (Events 4, 7, and 8). It only turned progressively from NE to NW during Event 6.

The minimal value of u_* appearing in Table 1 corresponds to the smallest vertical upward flux quantifiable by the gradient method. This minimum is 0.21 m s^{-1} for the whole measurement period, which is consistent with the threshold value (u_{*t}=0.22 m s^{-1}) yielded by the sand movement detector (saltiphone) operated on the same site (Dupont et al., 2018). Noteworthy, the maximal value achieved by u_* (Tab. 1) is always well above u_{*t}. This ensures that a wide range of variation of the erosion conditions was monitored during each one of the 8 events of this study.

The lowest roughness (Z_0~0.03 10^{-3} m) was measured during periods when the saltation was minimum. This value is in agreement with the surface roughness lengths measured in absence of saltation over flat bare surfaces (e.g., Marticorena et al. (2006) and references therein). When saltation develops, the range of variation of Z_0 is enlarged to about 3 10^{-3} m, which is also consistent with the values measured over flat bare eroding soils (Dupont et al., 2018; Gomes et al., 2003; Rajot et al., 2003; Shao et al., 2011; Sow et al., 2009). Indeed, in this case Z_0, which is then frequently referred to as the 'apparent roughness length', increases due to the presence of saltating particles and becomes larger than the actual roughness of the surface (Gillette et al., 1998; Owen, 1964; Raupach, 1991).

Table 1. Date, beginning and duration of the 8 dust events. The ranges of variation of u_*, and the wind direction (clockwise and with 0 to the north) are also indicated as well as the minimum Z_0 values.

Event details				u_* (m s^{-1})		Z_0 (10^{-3} m)	Wind Dir. (°)	
N	Date	Beg. (UTC)	Dur. (h)	Min	Max	Min	Min	Max
1	07/03/2017	10:20	7.2	0.21	0.40	0.03	288	348
2	08/03/2017	11:34	5.4	0.23	0.51	0.10	322	10
3	09/03/2017	08:16	8.4	0.28	0.47	0.16	318	344
4	15/03/2017	06:56	9.3	0.34	0.50	0.10	55	72
5	14/04/2017	10:20	5.6	0.23	0.33	0.03	273	292
6	16/04/2017	09:51	5.9	0.31	0.50	0.13	325	53
7	20/04/2017	07:31	9.1	0.27	0.40	0.05	32	69
8	02/05/2017	06:54	9.8	0.24	0.31	0.02	48	75

We also assessed the range of variability of the instability conditions during the 8 periods, by examining the range of variations of Ri (Fig. 3a), and its mechanical stress (u_*; Fig.

3b) and thermal ($\partial\theta/\partial z$; Fig. 3c) components. As expected for erosion events during which the wind gradient is by definition large, *Ri* remained small (-0.12 < *Ri* < 0.02) and its range of variation limited (Fig. 3a) as for instance during the 15 March event that remained constantly close to neutrality. However, with their slightly more negative *Ri*, some events such as 14 April and 2 May appear as relatively more unstable than the others. This instability results from the combination of a relatively strong negative thermal (Fig. 3c) and a weak wind (u_* < 0.32 m s^{-1}; Fig. 3b) gradients.

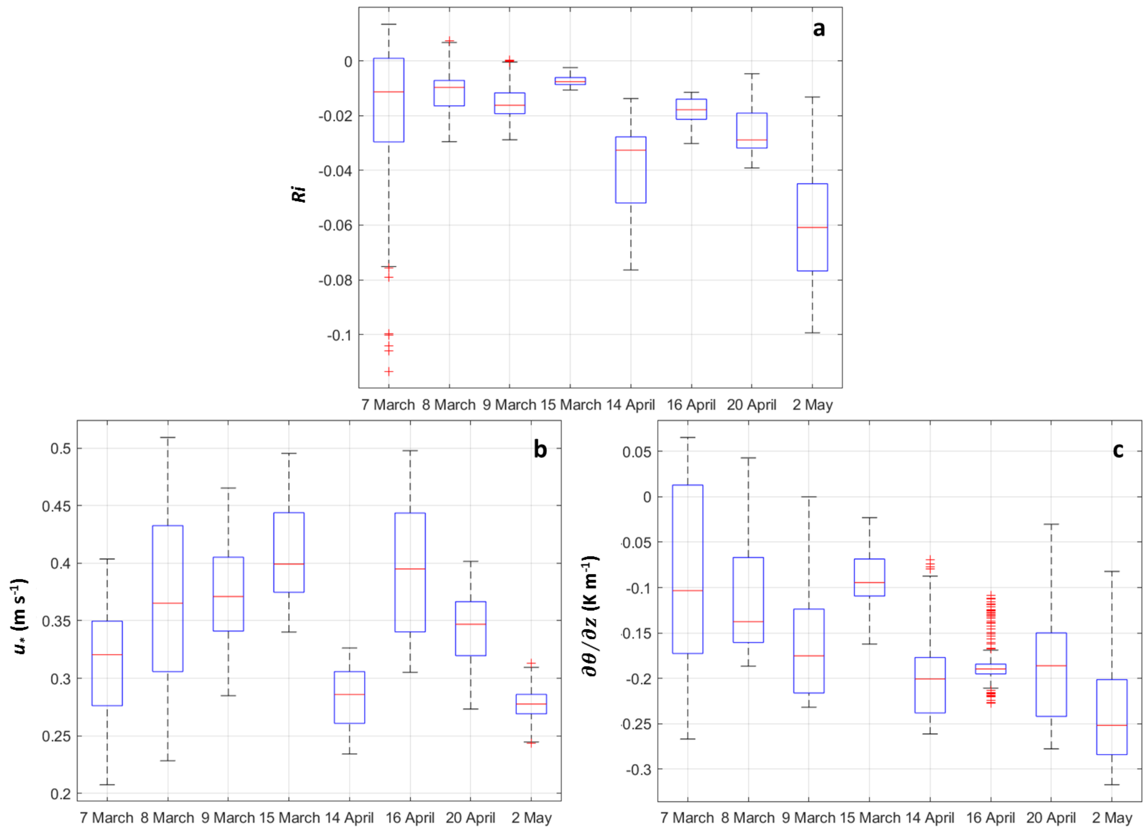

Figure 3. Boxplots of the variations of the Richardson number *Ri* (a), wind friction velocity u_* (b), and thermal gradient $\partial\theta/\partial z$ (c) during the 8 dust emission events. Whiskers are drawn from the ends of the interquartile ranges to the furthest observations within the whisker length that is equal to 1.5 times the interquartile range at a maximum. Values beyond this limit (red crosses) are defined as outliers.

3.2 Influence of the stability conditions on the vertical dust flux

3.2.1. Vertical number dust flux

Figure 4a illustrates the variations of $F_{d,n}$ with u_* for each of the eight dust emission events. $F_{d,n}$ increased from nearly 0 to more than 6.10^7 particles m^{-2} s^{-1} when u_* increased from u_{*t} (0.21 m s^{-1}) to 0.51 m s^{-1}. As expected from the smallness of the gravitational settling flux (F_s), the general behavior of the diffusive flux (F_d) is consistent with the power law (Equation

(1)) describing the evolution of F_v with u_*. The constants C and n (7.1 10^8 and 2.90, respectively) were determined by the means of a least square iterative routine and the adjustment found to be satisfactory (slope=0.93, vertical intercept=1.73 10^6, R^2=0.76, N=3135), thus confirming that the wind friction velocity is the main driver of the vertical dust flux. However, a relatively large scatter of the experimental data around the power law can still be observed. For instance, for similar u_* in the range 0.4-0.5 m s^{-1}, $F_{d,n}$ is approximately 2 to 3 times larger on 9 March than on 15 March. This shows that u_* is not the sole predictor of the magnitude of the vertical dust flux.

In the introduction, we hypothesized that stability conditions could have an effect on the efficiency of the vertical transfer of the emitted dust. This assumption is roughly confirmed by our measurements. Indeed, when the $F_{d,n}$ data acquired in thermally 'unstable' conditions (i.e., when $\partial\theta/\partial z$ < -0.2 K m^{-1}) are distinguished from the others (Fig. 4b), it appears that the total vertical dust number flux is quasi-systematically above the value predicted by the average 'power' law even if the two categories seem to converge at large u_* (> 0.45 m s^{-1}), which is to say when the production of turbulence by wind shear is likely to predominate largely over that by thermal instability.

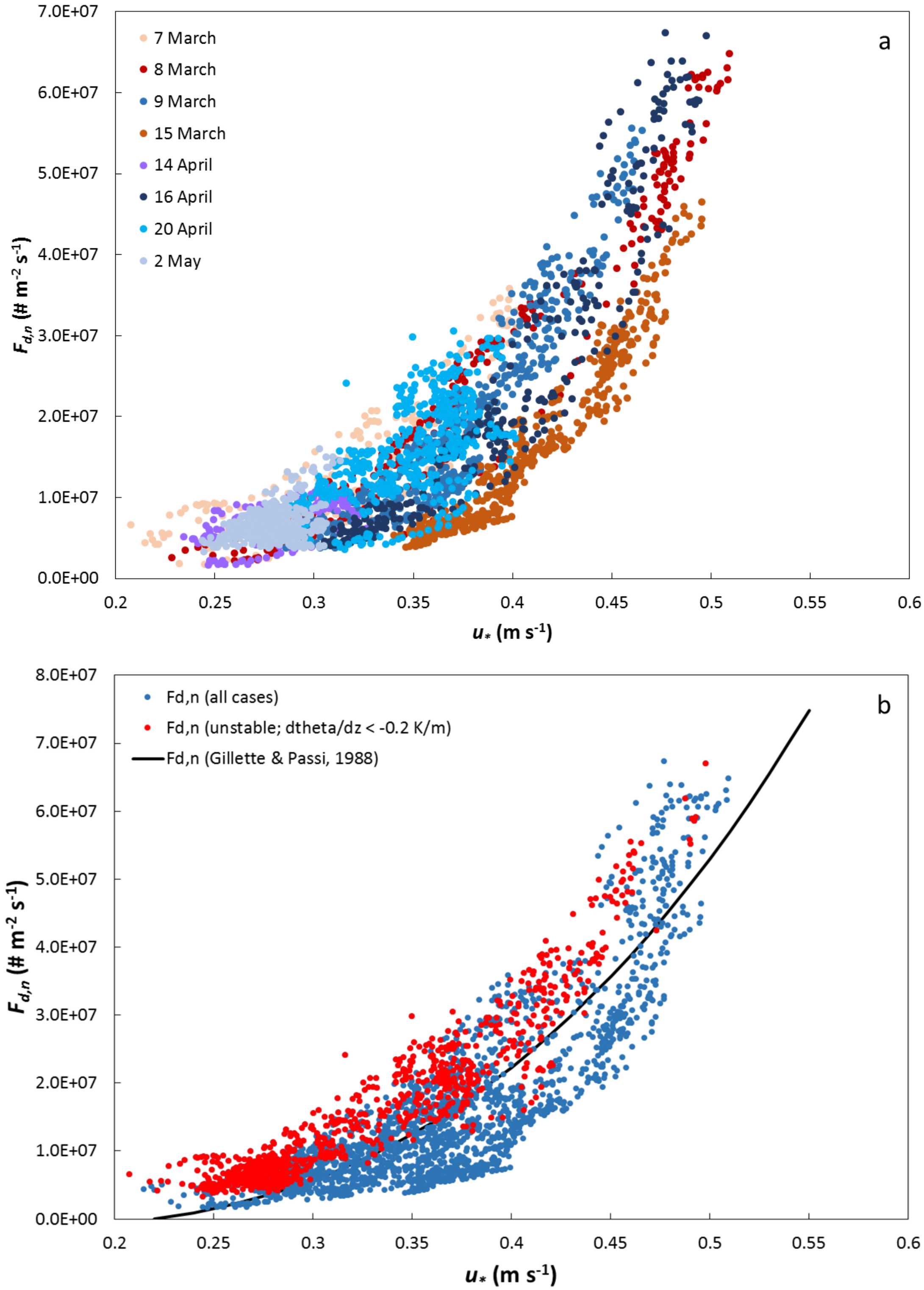

Figure 4. Total number vertical dust flux ($F_{d,n}$ in particles m^{-2} s^{-1}) as a function of the wind friction velocity (u_*, in m s^{-1}) during the 8 wind erosion events (a), and sorted according to their thermal stability (b) (red points were acquired when $\partial\theta/\partial z$ was < -0.2 K m^{-1}; the blue points represent the remainder of the dataset). In (b), the black solid line corresponds to the adjustment of the "power law" of Gillette & Passi (1988) to the entire dataset (see coefficients in the text).

3.2.2. Size distribution of the vertical number dust flux

Figure 5 displays the size distributions of the vertical number dust flux averaged over the duration of each dust event. These size distributions appear to be mainly bi-modal with one fine mode centered on 0.6 µm and another coarser and more variable one around 1.5 µm (Fig. 5). The relative proportions of these two modes vary from one event to the other. For instance, the coarse mode is more abundant during events 1 (7 March), 2 (8 March) and 4 (15 March), than during the other ones. As denoted by the length of the error bars (standard error of the mean), the variability of the size-distribution inside a given event is quite large.

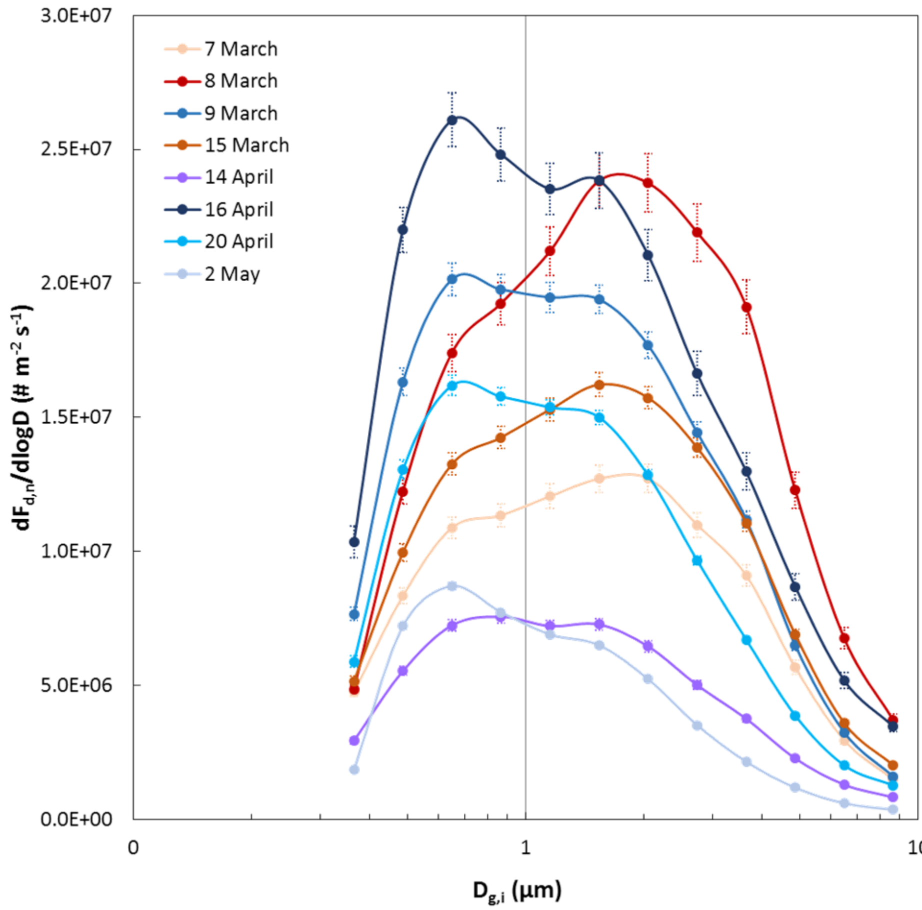

Figure 5. Average size-resolved number vertical dust flux ($F_{d,n}$ in particles m^{-2} s^{-1}) for the 8 dust emission events of this study. Vertical dotted bars represent the standard error of the mean.

Figure 6 presents a comparison of the size distributions of the vertical number dust flux measured during the 8 dust events of the WIND-O-V's 2017 campaign with those measured by Fratini et al. (2007) in northern China (Gobi desert) and by Sow et al. (2009) in Niger (Sahel) during the Special Observing Periods of the AMMA international program. It can be seen that the magnitude of the dust flux measured during the WIND-O-V's 2017 campaign compares to those measured by Fratini et al. (2007) and by Sow et al. (2009) during Monsoon Events (ME1 and ME4), but is from one order of magnitude lower than those measured during Convective Events (CE4). Part of these differences can be explained by the range of variation of u_*: the high friction velocity class defined by Fratini et al. (2007) refers to the peak of the dust event, i.e., to $0.45 < u_* < 0.60$ m s^{-1}, and during the monsoon events ME1 and ME4 u_* ranged from 0.40 to 0.50 m s^{-1}. In both cases, it corresponds to the range of variation of u_* measured during the 8 dust events of the WIND-O-V's 2017 campaign (Tab. 1). Conversely, u_* reached values as high as 0.8 m s^{-1} during the CE4 event reported by Sow et al. (2009).

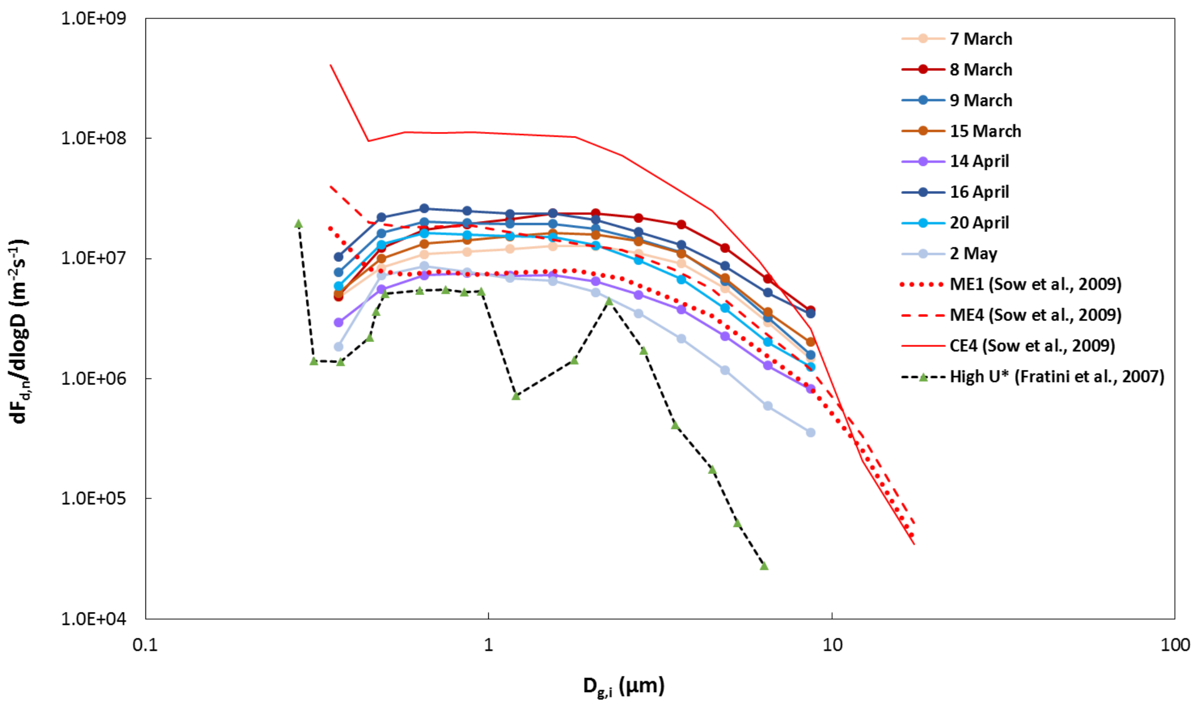

Figure 6. Average size-resolved number vertical dust flux ($F_{d,n}$ in particles m^{-2} s^{-1}) for the 8 dust emission events of this study (7 March to 2 May), for the ME1, ME4 and CE4 events from Sow et al. (2009), and for the high u_* event from Fratini et al. (2007).

As a first clue for understanding the variability of the size-distribution, it can be noted that the events whose average vertical fluxes are the richest in fine particles (16 April, 2 May…) are also globally the most unstable (see their range of R_i and $\partial\theta/\partial z$ in Fig. 3). Therefore, it seems necessary to study in more detail not only the influence of Ri on the size distribution of $F_{d,n}$, but also those of its u_* and $\partial\theta/\partial z$ components. For doing so, we have calculated the cumulative proportions of 'fine' and 'coarse' (with a separation set arbitrarily at D = 1.78 µm after visual observation of Fig. 5) particles in the vertical flux and plotted them as a function of Ri (Fig. 7a), u_* (Fig. 7b) and $\partial\theta/\partial z$ (Fig. 7c).

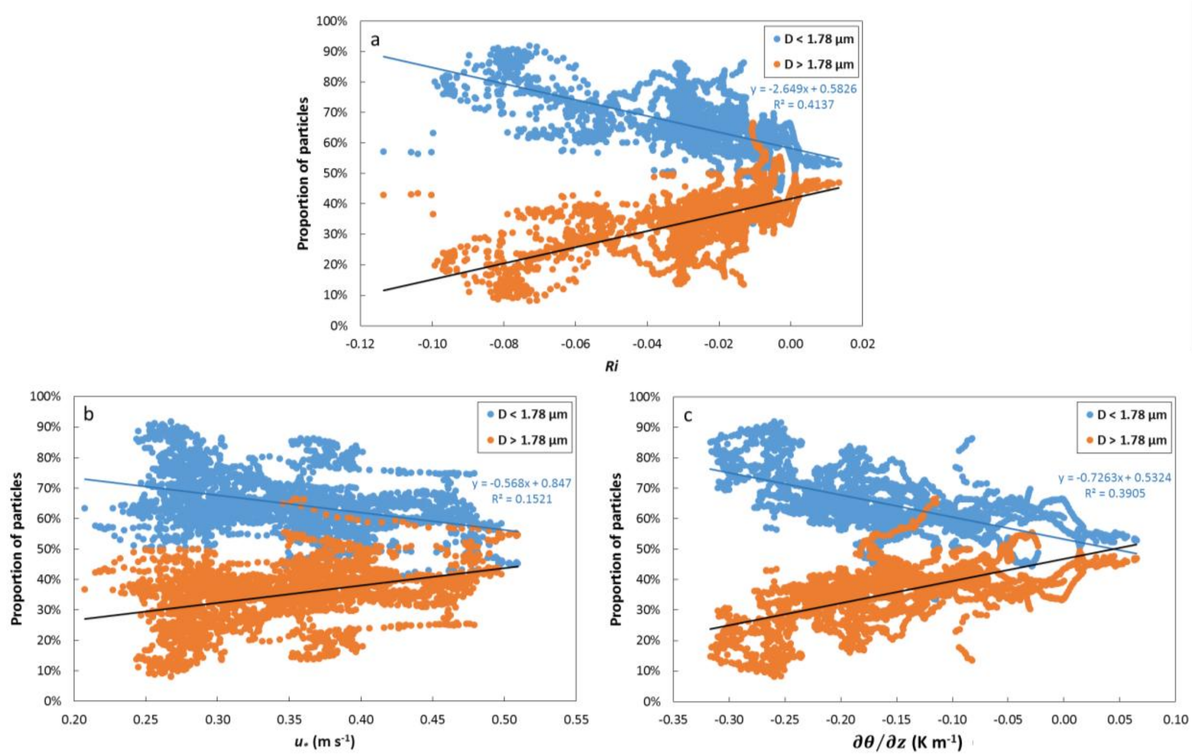

Figure 7. Evolution of the proportions of particles with diameter < 1.78 µm (blue dots – N = 3135) and > 1.78 µm (orange dots – N = 3135) as a function of the Richardson number *Ri* (a), the wind friction velocity u_* (b), and the thermal gradient $\partial\theta/\partial z$ (c). All the measurements performed during the 8 dust emission events were considered. The linear regression line and the quality of the regression (R^2) are also reported.

The relative proportion of fine particles and that of the coarse particles (which is simply its complementary) clearly evolve linearly (R^2=0.41) with *Ri* (Fig. 7a). Though significant, the correlation with u_* is weaker (R^2=0.16) (Fig. 7b). Thus, it can be concluded that rather than u_* this is mostly the thermal component of *Ri* (namely, $\partial\theta/\partial z$) that controls the proportions of fine and coarse particles in the vertical flux (Fig. 7c). This influence of the thermal instability on the size-distribution can be further evidenced (Fig. 8) by sorting all the available data in categories of increasing instability on the basis of their $\partial\theta/\partial z$ values. The limits of the $\partial\theta/\partial z$ classes were chosen in order to 1) cover the full range of variability of the thermal gradient, and 2) ensure that a representative number of cases (*N*, reported in Table 2) were present in each of these categories. It clearly appears (Fig. 8) that the proportion of particles smaller (larger) than 1.78 µm in the vertical flux increases (decreases) with the thermal instability.

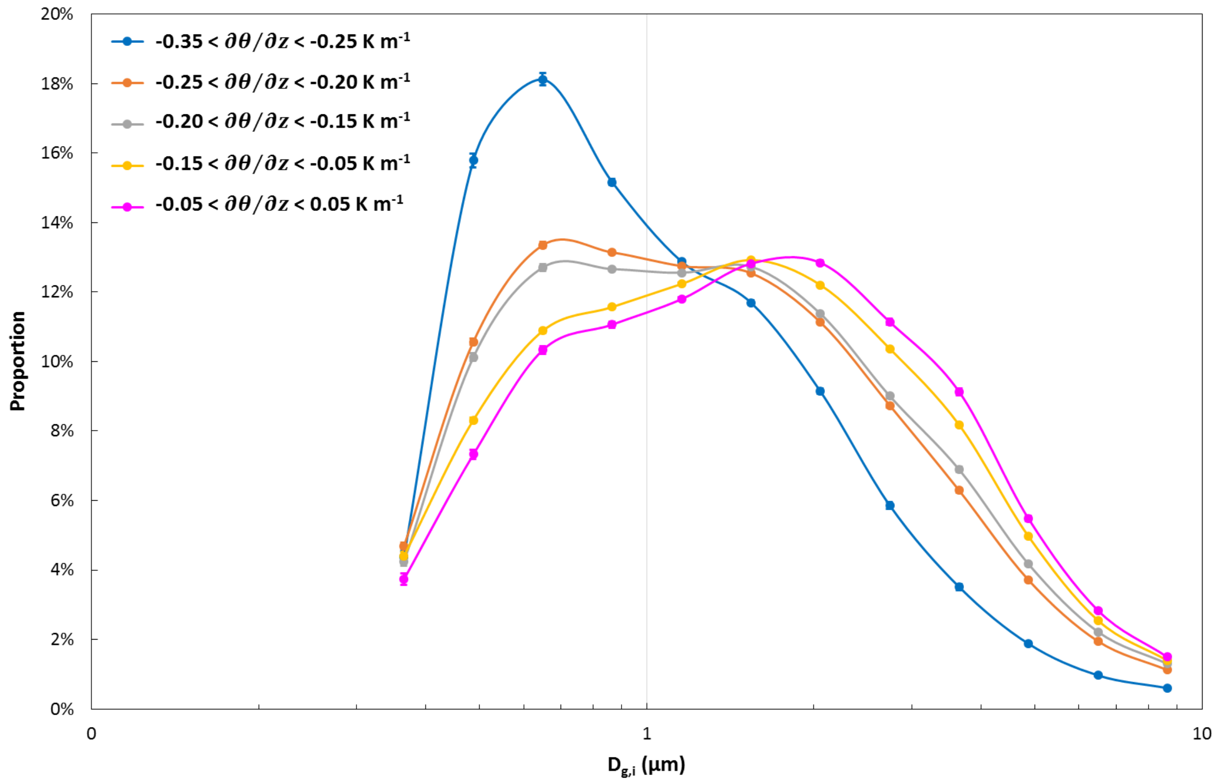

Figure 8. Relative size-resolved number emission flux for different classes of thermal stability. Vertical dotted bars represent the standard error of the mean.

3.2.3. Modes of the vertical dust flux size distribution

In order to characterize more precisely the evolution of the size-distribution, we have determined the geometrical mean diameters (gmd), geometrical standard deviations (gsd), and proportions of the two lognormally distributed populations of particles present in the 5 normalized vertical fluxes of Fig. 8. The quality of the deconvolution is excellent (R^2>0.99, slope =1.00±0.02, vertical intercept < 0.05%), and the gmd, gsd and proportions of the two particles populations are reported in Table 2. The size characteristics of the fine mode (gmd = 0.58±0.02 µm and gsd = 1.37±0.10) are independent of the thermal stability. Its proportion is maximal (26.2%) in the most unstable category ($-0.35 < \partial\theta/\partial z < -0.25$), but the evolution of the size-distribution is in large part explained by changes of the coarse mode. Indeed, its breadth remains rather constant (gsd = 2.12±0.13) but its gmd decreases continuously from 1.93 µm in quasi-neutral conditions to 1.20 µm in the most unstable ones. This progressive shift of the gmd of the coarse mode towards finer diameters is responsible for the increase of the relative proportion of submicron particles in the vertical flux.

After conversion of the number distributions into volume ones, the proportion of the total volume occupied by the submicron mode is found to be less than 2% (Table 2) and therefore negligible. Except in the most unstable case when it is significantly smaller (4.62 µm), the gmd of the coarse mode is close to the upper limit of the measuring capacity of the OPC (10 ± 1µm).

Table 2. Results of the deconvolution of the number size-resolved dust emission fluxes for different classes of thermal stability. In each class, the dust emission flux can be considered as a mixture of 2 lognormally distributed populations whose geometric standard deviation (gsd), geometric mean diameters (gmd, in µm), and proportions (%) are reported. The number of points N in each class is reported in parenthesis. The gmd and proportions obtained after number to mass conversion are also indicated.

		$-0.35 < \frac{\partial\theta}{\partial z} < -0.25$ *(N = 415)*		$-0.25 < \frac{\partial\theta}{\partial z} < -0.20$ *(N = 600)*		$-0.20 < \frac{\partial\theta}{\partial z} < -0.15$ *(N = 827)*		$-0.15 < \frac{\partial\theta}{\partial z} < -0.05$ *(N = 992)*		$-0.05 < \frac{\partial\theta}{\partial z} < 0.05$ *(N = 301)*	
		Pop. 1	Pop. 2	Pop. 1	Pop. 2	Pop. 1	Pop. 2	Pop. 1	Pop. 2	Pop. 1	Pop. 2
gsd		1.3	2.0	1.3	2.2	1.3	2.3	1.5	2.1	1.5	2.0
gmd (µm)	in number	0.57	1.20	0.58	1.39	0.58	1.43	0.57	1.71	0.61	1.93
	in mass	0.67	4.62	0.74	9.39	0.71	10.49	0.88	9.71	0.99	8.70
%	in number	26.2	75.0	15.5	88.1	13.2	90.7	18.3	84.8	22.5	79.9
	in mass	0.6	99.4	0.1	99.9	1.8	98.2	0.1	99.9	0.2	99.8

4 Discussion

Because of the constant flux layer assumption underlying the gradient method, the diffusive flux F_d is supposed to represent the emission flux (F_{emiss}), which is to say the vertical upward flux of particles leaving the surface from which they were released. Our results show that both the intensity and size distribution of F_d measured between 2.04 and 4.10 m above the ground depend on the thermal structure of the SBL.

It is physically difficult to conceive that the magnitude and size-distribution of the flux at the immediate interface between the soil and the atmosphere might be affected by the thermal stratification of the air layer above it. Thus, our results strongly suggest that the vertical temperature gradient alters significantly the efficiency of the transfer of particles from the surface to higher altitudes and that this effect is size-dependent.

This contradicts two fundamental assumptions of the gradient method, namely that 1) the diffusion coefficient (K_p) of Equation (2) is independent of D_p, which is to say that all particles with diameters smaller than approximately 10 µm have the same ability to follow the movements of the air-masses in which they are embedded (Gillette et al., 1972), and 2) it is possible to account for the effect of thermal stratification on the vertical transport of these fine particles by using the momentum stability functions.

4.1 Dependence of K_p on particle size in neutral conditions

K_p is expected to depend on particle size even in neutral conditions because of the trajectory crossing effect. This theory proposed by Csanady (1963) states that because of their inertia large particles respond more slowly to turbulent fluctuations than smaller ones, are less apt to follow the trajectories of the air parcels in which they were initially embedded, and are thus more prone to shift from one turbulent eddy to another. The author suggested that the effect should be significant for particles larger than about 20 µm in highly turbulent conditions but also for smaller particles in less turbulent conditions. Later on, Wang & Stock (1993) showed that for coarse particles K_p should not only decrease with particle size because of the trajectory crossing effect but also depend on the intensity of the turbulence (the lower this intensity, the larger the deviation of K_p from the eddy-diffusivity of the air-parcels). In summary, K_p should depend not only on particle size but also on the structure of the turbulence. Unfortunately, for lack of experimental data it has not been possible so far to test the applicability of these results to particles smaller than 20 µm.

4.2 Dependence of K_p on particle size in thermally unstable conditions.

Our results showed that, though not exclusively, the influence of atmospheric instability on the characteristics of the vertical flux was more strongly felt during the 14 April and 2 May events, which is to say during events characterized by the lowest u_* and the strongest thermal gradients. These conditions correspond to the so-called 'Unstable Very Close to Neutral' (UVCN) regime studied by Smedman et al. (2007). These authors showed that in such situations, the eddy structure in the surface layer was considerably altered by the weak buoyancy, which in turn enhanced the efficiency of the heat and water vapor upward transfers. As seen above, the finest particles are more apt than the coarsest ones to follow the air-parcels movements and could thus be more liable to benefit from the apparition of new turbulent structures favoring their vertical transport from the surface to higher atmospheric levels. Note that this interpretation is also consistent with the theory of Wang & Stock (1993) extrapolated to diameters < 10 µm. Finally, our experimental results are also in good qualitative agreement with the theory proposed by Freire et al. (2016) for establishing a link between the emission flux at the surface and the vertical profile of particles concentration in the SBL. These authors hypothesized that the effect of atmospheric stability should be incorporated in the parameterization of the eddy diffusivity of the particles. In their theory, the dependence to size is taken into account by the means of the trajectory-crossing effect, which is tantamount to considering that K_p decreases slowly with size, and they thus conclude from their idealized LES simulations that the effect of gravitational settling should be only secondary to that of stability. Our own results confirm the importance of atmospheric stability but also suggest that in natural conditions the dependence of this effect on particle size could be larger than considered in the current theories.

In order to quantify the effect of thermal instability on the size-distribution of the vertical flux, we examined the evolution with $\partial\theta/\partial z$ of its deviations from the neutral case. Practically, we calculated the ratio of the relative contributions of each size class in non-neutral and near-neutral ($-0.05<\partial\theta/\partial z<0.05$°C m^{-1}) conditions and plotted this ratio as a function of $\partial\theta/\partial z$. Figure 9 illustrates the results for a fine (0.49 µm), an intermediate (1.15 µm), and a coarse (3.65 µm) size class. In spite of some scatter, a linear behavior is observed in the three cases. By definition of the ratio, the vertical intercept that represents its value in neutral conditions is equal to 1. The slope (hereinafter noted A) denotes the sensitivity of the proportion of one given size-class to thermal stratification. Consistent with the enrichment of the dust flux in fine particles in thermally unstable conditions, A is found to be negative for the fine class and positive for the coarse one. For particles with $D_{g,i}$ between 1.15 and 1.54 µm, A is almost nil, which means that, in the vertical dust flux, the proportion of particles in this size range is independent of $\partial\theta/\partial z$. The increase of A with the diameter of the particles (Fig. 9b) can be quite well (slope=0.99, b=0.002, R^2=0.99, n=11) represented by the following expression:

$$A = A_{lim}(1 - B\exp(-k\,D_p)) \tag{9}$$

The values of B and k are 4.56 (unit-less) and 1.11 (µm^{-1}), respectively. A_{lim} is the limit towards which A tends above a diameter of approximately 4 µm. Its numerical value is 1.54. Note that the fact that the dependence of A to size is notable only below 4 µm and larger for the smallest size-classes, confirms again that the very fine particles are the most sensitive to the modification of the turbulence structure resulting from a moderately unstable thermal stratification.

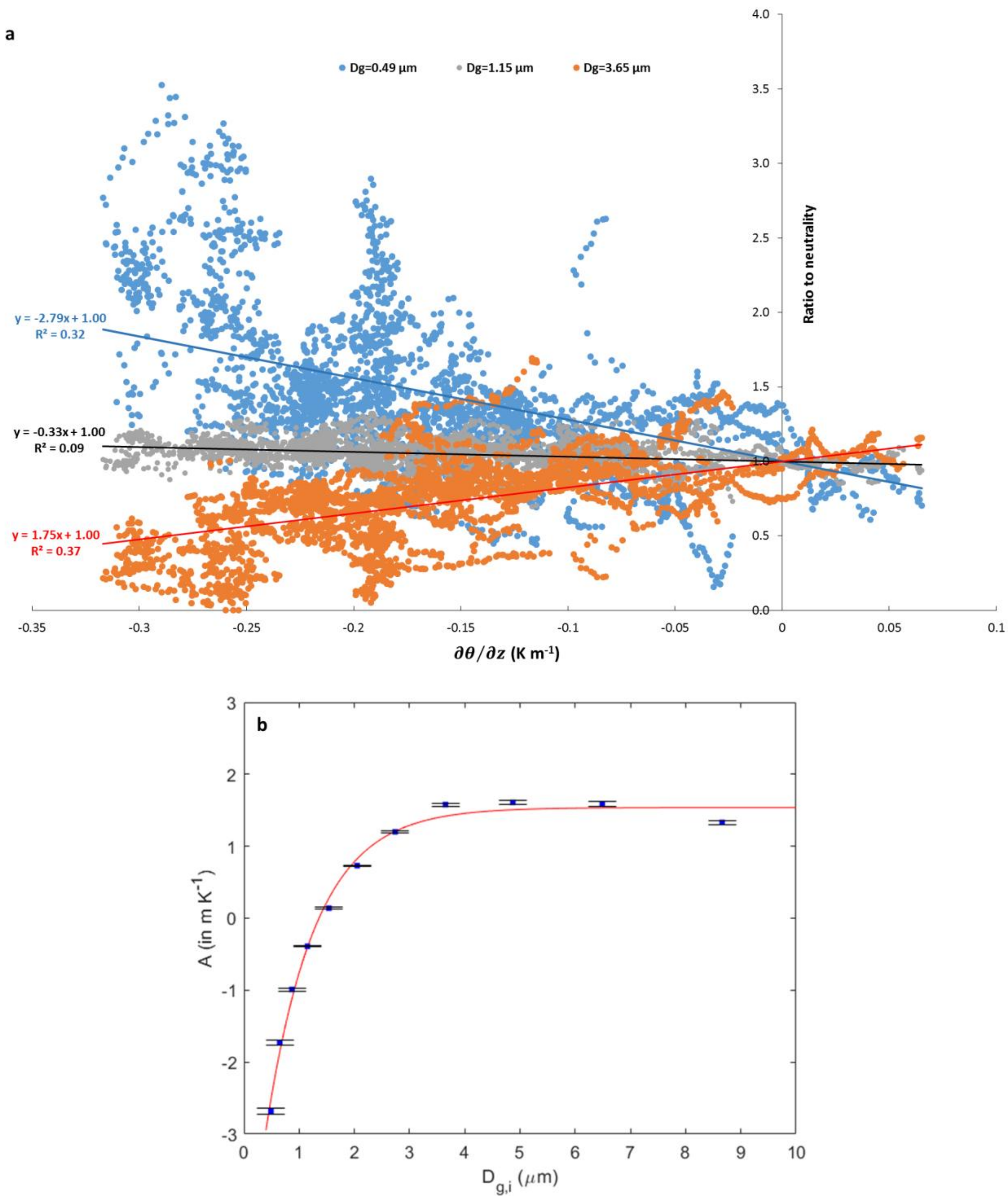

Figure 9. (a) Influence of thermal instability ($\partial\theta/\partial z$) on the proportions of particles of three different size-classes (0.49, 1.15, and 3.65 µm) in the vertical flux (the reference is the neutral case), and (b) evolution with particle size of the slopes of the linear trends obtained in each size-class (blue squares and the associated standard deviation in black). In the latter case, the solid red line is the mathematical adjustment (Eq. 9) to the measurements.

4.3 Implications for the modeling of the vertical flux.

Independently of the physical scheme used to estimate them, dust emission models usually assume that the flux of particles released from the surface (F_{emiss}) can be characterized by its intensity and relative size-distribution and that the latter is either constant (Kok, 2011b) or varying with wind speed (Alfaro & Gomes, 2001; Shao, 2001) but the size distribution of the vertical flux is simply derived from that of $F_{emiss.}$ The results of our study emphasizes the importance of taking into account the thermal stratification of the surface layer in this derivation. Practically, this could be achieved by using transfer functions similar to that of Equation (9) allowing to express the size-distribution of the vertical flux in unstable conditions to that of neutral conditions.

5 Summary and conclusions

The vertical dust flux was measured during 8 wind erosion events over a flat sandy field in southern Tunisia. This allowed documenting the impact of a large variety of dynamical conditions on the magnitude of the number vertical flux and its size-distribution. During the first events of the WIND-O-V's 2017 experimental campaign, the wind strength tended to be globally larger and the thermal stratification of the SBL closer to thermal neutrality than later on. These differences had a direct impact on the magnitude and number size-distribution of the vertical dust flux measured by the gradient method between 2.04 and 4.10 m above the surface. The size-distribution was relatively richer in supermicron particles during the thermally neutral periods of the events, whereas the proportion of submicron ones increased in unstable conditions. Note that the discussion provided as supplementary material to this paper shows that the relatively short fetch of our experimental plot can be ruled out as a primary explanation for the enrichment in fine particles. Therefore, our results are in contradiction with two of the assumptions of the gradient method, namely 1) that the turbulent eddy coefficient of the particles smaller than 10 µm should be the same as that of the transport of the air-mass momentum, and therefore independent of the particles size, and 2) that the stability functions commonly used to account for the thermal stratification of the surface layer should be directly applicable to the vertical transport of dust particles.

Fundamentally, this means that the size-distributions determined from in-situ measurements performed at a height of a few meters do not necessarily reflect directly the actual distribution of the particles produced by sandblasting at the surface. According to the results of this study, only the size-distributions measured in, or very close to, neutral conditions are expected to approach this size-distribution. This could also explain that the size-distributions measured in this study seem to be controlled more by thermal instability than by u_* and that the effect of the latter parameter, though evidenced in wind-tunnel experiments (Alfaro et al., 1997, 1998), appears as one of second order magnitude in natural conditions.

Finally, our results stress the importance of documenting carefully not only the evolution of u_* but also those of the vertical thermal gradient when interpreting the variations of the size-distribution of the vertical flux measured over an eroding field. In our case, it has been possible to find an empirical correlation between this size-distribution and the thermal structure of the SBL but it is not certain whether similar corrections could be applied to any type of eroding surface. More experimental studies performed in other source areas are clearly necessary to address this question and over plots with a longer fetch would clearly be necessary to address this question. New theoretical developments would also be urgently needed to explain the larger than expected dependence to size of the vertical entrainment of fine dust particles in unstable SBL.

Acknowledgments and Data

The authors acknowledge the support of the French Research Agency (ANR) under the grant ANR-15-CE02-0013 (project WIND-O-V). The authors would like to thank: (i) Houcine Khatteli, Director of the Institut des Régions Arides (IRA) of Médenine, for the constant support of IRA in all research related to wind erosion, and in particular for giving us access to the Dar Dhaoui's experimental range and for the IRA's logistic help during the whole experiment to ensure the success of the campaign, (ii) the guards of the experimental stations (Noureddine Boukhli, Mokhtar Elghoul and Mousbah Elghoul) for their constant help and surveillance of the experimental system, (iii) Jean Marc Bonnefond, and Didier Garrigou from the Interactions Sol Plante Atmosphère laboratory (UMR INRA 1391) for their help in the installation of the experimental device, and (iv) Mme Marguerite Perrey from the Chrono-environnement laboratory (UMR CNRS 6249) for the measurement of the totally dispersed soil distribution. The data used in this manuscript are available for download for research and educational purposes at the web link http://www.lisa.univ-paris12.fr/fr/donnees maintained by Laboratoire Interuniversitaire des Systèmes Atmosphériques.

References

Abbasi, A., Annor, F. O., & van de Giesen, N. (2017). Effects of atmospheric stability conditions on heat fluxes from small water surfaces in (semi-)arid regions. *Hydrological Sciences Journal*, *62*(9), 1422–1439. https://doi.org/10.1080/02626667.2017.1329587

Alfaro, S. C., & Gomes, L. (2001). Modeling mineral aerosol production by wind erosion: Emission intensities and aerosol size distributions in source areas. *Journal of Geophysical Research*, *106*(D16), 18075–18084.

Alfaro, S. C., Gaudichet, A., Gomes, L., & Maillé, M. (1997). Modeling the size distribution of a soil aerosol produced by sandblasting. *Journal of Geophysical Research*, *102*(10), 11239–11249.

Alfaro, S. C., Gaudichet, A., Gomes, L., & Maillé, M. (1998). Mineral aerosol production by wind erosion: aerosol particle sizes and binding energies. *Geophysical Research Letters*, *25*(7), 991–994.

Arya, S. P. (1988). *Introduction to micrometeorology*. New York: Elsevier.

Bagnold, R. A. (1941). *The physics of blown sand and desert dunes*. London: Methuen.

Boucher, O., Randall, D., Artaxo, P., Bretherton, C., Feingold, G., Forster, P., et al. (2013). Clouds and aerosols. In *Climate Change 2013: The Physical Basis. Contribution of Working Group I to the Fifth Assessment*

Report of the Intergovernmental Panel on Climate Change (Cambridge University Press). Cambridge, United Kingdom and New York, NY, USA: T. F. Stocker, D. Qin, G.-K. Plattner, M. Tignor, S. K. Allen, J. Boschung, A. Nauels, Y. Xia, V. Bex, and P. M. Midgley.

Businger, J. A. (1986). Evaluation of the accuracy with which dry deposition can be measured with current micrometeorological techniques. *Journal of Climate and Applied Meteorology*, *25*, 1100–1124.

Businger, J. A., Wyngaard, J. C., Izumi, Y., & Bradley, E. F. (1971). Flux-profile relationships in the atmospheric surface layer. *Journal of the Atmospheric Sciences*, *28*, 181–189.

Chatenet, B., Marticorena, B., Gomes, L., & Bergametti, G. (1996). Assessing the microped size distributions of desert soils erodible by wind. *Sedimentology*, *43*, 901–911.

Chou, C., Formenti, P., Maille, M., Ausset, P., Helas, G., Harrison, M., & Osborne, S. (2008). Size distribution, shape, and composition of mineral dust aerosols collected during the African Monsoon Multidisciplinary Analysis Special Observation Period 0: Dust and Biomass-Burning Experiment field campaign in Niger, January 2006. *Journal of Geophysical Research*, *113*, D00C10. https://doi.org/10.1029/2008JD009897

Csanady, G. T. (1963). Turbulent diffusion of heavy particles in the atmosphere. *Journal of the Atmospheric Sciences*, *20*, 201–208.

DeMott, P. J., Cziczo, D. J., Prenni, A. J., Murphy, D. M., Kreidenweis, S. M., Thomson, D. S., et al. (2003). Measurements of the concentration and composition of nuclei for cirrus formation. *Proceedings of the National Academy of Sciences*, *100*(25), 14655–14660. https://doi.org/10.1073/pnas.2532677100

Duce, R. A., Liss, P. S., Merrill, J. T., Atlas, E. L., Buat-Menard, P., Hicks, B. B., et al. (1991). The atmospheric input of trace species to the world ocean. *Global Biogeochemical Cycles*, *5*(3), 193–259.

Dupont, S., Rajot, J.-L., Labiadh, M., Bergametti, G., Alfaro, S. C., Bouet, C., et al. (2018). Aerodynamic parameters over an eroding bare surface: Reconciliation of the Law of the Wall and Eddy Covariance determinations. *Journal of Geophysical Research: Atmospheres*, *123*(9), 4490–4508. https://doi.org/10.1029/2017JD027984

Dupont, S., Rajot, J. -L., Labiadh, M., Bergametti, G., Lamaud, E., Irvine, M. R., et al. (2019). Dissimilarity between dust, heat, and momentum turbulent transports during aeolian soil erosion. *Journal of Geophysical Research: Atmospheres*, *124*(2), 1064–1089. https://doi.org/10.1029/2018JD029048

Dyer, A. J. (1974). A review of flux-profile relationships. *Boundary-Layer Meteorology*, *7*(3), 363–372. https://doi.org/10.1007/BF00240838

Dyer, A. J., & Hicks, B. B. (1970). Flux-gradient relationships in the constant flux layer. *Quarterly Journal of the Royal Meteorological Society*, *96*(410), 715–721. https://doi.org/10.1002/qj.49709641012

Frangi, J.-P., & Richard, D. C. (2000). The WELSONS experiment: overview and presentation of first results on the surface atmospheric boundary-layer in semiarid Spain. *Annales Geophysicae*, *18*, 365–384.

Fratini, G., Ciccioli, P., Febo, A., Forgione, A., & Valentini, R. (2007). Size-segregated fluxes of mineral dust from a desert area of northern China by eddy covariance. *Atmospheric Chemistry and Physics*, *7*(11), 2839–2854.

Freire, L. S., Chamecki, M., & Gillies, J. A. (2016). Flux-profile relationship for dust concentration in the stratified atmospheric surface layer. *Boundary-Layer Meteorology*, *160*(2), 249–267. https://doi.org/10.1007/s10546-016-0140-2

Gillette, D. A. (1977). Fine particle emissions due to wind erosion. *Transactions of the American Society of Agricultural Engineers*, *20*, 890–897.

Gillette, D. A. (1981). Production of dust that may be carried great distances. In *Desert dust: Origin, characteristics, and effect on man* (Vol. 186, pp. 11–26). Péwé, T. L.

Gillette, D. A., & Passi, R. (1988). Modeling dust emission caused by wind erosion. *Journal of Geophysical Research*, *93*(D11), 14233–14242.

Gillette, D. A., & Walker, T. R. (1977). Characteristics of airborne particles produced by wind erosion of sandy soil, high plains of west Texas. *Soil Science*, *123*(2), 97–110.

Gillette, D. A., Blifford Jr., I. H., & Fenster, C. R. (1972). Measurements of aerosol size distributions and vertical fluxes of aerosols on land subject to wind erosion. *Journal of Applied Meteorology*, *11*, 977–987.

Gillette, D. A., Fryrear, D. W., Xiao, J. B., Stockton, P., Ono, D., Helm, P. J., et al. (1997). Large-scale variability of wind erosion mass flux rates at Owens Lake 1. Vertical profiles of horizontal mass fluxes of wind-eroded particles with diameter greater than 50 µm. *Journal of Geophysical Research*, *102*(D22), 25977–25987.

Gillette, D. A., Marticorena, B., & Bergametti, G. (1998). Change in the aerodynamic roughness height by saltating grains: Experimental assessment, test of theory, and operational parameterization. *Journal of Geophysical Research*, *103*(D6), 6203–6209. https://doi.org/10.1029/98JD00207

Golder, D. (1972). Relations among stability parameters in the surface layer. *Boundary-Layer Meteorology*, *3*(1), 47–58.

Gomes, L., Bergametti, G., Coudé-Gaussen, G., & Rognon, P. (1990). Submicron desert dusts: A sandblasting process. *Journal of Geophysical Research*, *95*(D9), 13927–13935.

Gomes, L., Rajot, J. L., Alfaro, S. C., & Gaudichet, A. (2003). Validation of a dust production model from measurements performed in semi-arid agricultural areas of Spain and Niger. *Catena*, *52*(3–4), 257–271. https://doi.org/10.1016/S0341-8162(03)00017-1

Greeley, R., & Iversen, J. D. (1985). *Wind as a geological process on Earth, Mars, Venus and Titan* (Cambridge University Press). Cambridge - London - New York - New Rochelle - Melbourne - Sydney.

Hashizume M., Ueda K., Nishiwaki Y., Michikawa T., & Onozuka D. (2010). Health effects of Asian dust events: a review of the literature. *Japanese Journal of Hygiene*, *65*(3), 413–421. https://doi.org/10.1265/jjh.65.413

Hicks, B. B. (1976). Wind profile relationships from the 'Wangara' experiment. *Quarterly Journal of the Royal Meteorological Society*, *102*(433), 535–551. https://doi.org/10.1002/qj.49710243304

Ishizuka, M., Mikami, M., Leys, J. F., Shao, Y., Yamada, Y., & Heidenreich, S. (2014). Power law relation between size-resolved vertical dust flux and friction velocity measured in a fallow wheat field. *Aeolian Research*, *12*, 87–99. https://doi.org/10.1016/j.aeolia.2013.11.002

Jickells, T. D., An, Z. S., Andersen, K. K., Baker, A. R., Bergametti, G., Brooks, N., et al. (2005). Global iron connections between desert dust, ocean biogeochemistry, and climate. *Science*, *308*(5718), 67–71. https://doi.org/10.1126/science.1105959

Kandler, K., Benker, N., Bundke, U., Cuevas, E., Ebert, M., Knippertz, P., et al. (2007). Chemical composition and complex refractive index of Saharan Mineral Dust at Izaña, Tenerife (Spain) derived by electron microscopy. *Atmospheric Environment*, *41*(37), 8058–8074. https://doi.org/10.1016/j.atmosenv.2007.06.047

Kandler, K., Schütz, L., Deutscher, C., Ebert, M., Hofmann, H., Jäckel, S., et al. (2009). Size distribution, mass concentration, chemical and mineralogical composition and derived optical parameters of the boundary layer aerosol at Tinfou, Morocco, during SAMUM 2006. *Tellus B: Chemical and Physical Meteorology*, *61B*(1), 32–50. https://doi.org/10.1111/j.1600-0889.2008.00385.x

Klaver, A., Formenti, P., Caquineau, S., Chevaillier, S., Ausset, P., Calzolai, G., et al. (2011). Physico-chemical and optical properties of Sahelian and Saharan mineral dust: in situ measurements during the GERBILS campaign. *Quarterly Journal of the Royal Meteorological Society*, *137*(658), 1193–1210. https://doi.org/10.1002/qj.889

Klose, M., & Shao, Y. (2013). Large-eddy simulation of turbulent dust emission. *Aeolian Research*, *8*, 49–58. https://doi.org/10.1016/j.aeolia.2012.10.010

Kok, J. F. (2011a). A scaling theory for the size distribution of emitted dust aerosols suggests climate models underestimate the size of the global dust cycle. *Proceedings of the National Academy of Sciences*, *108*(3), 1016–1021.

Kok, J. F. (2011b). Does the size distribution of mineral dust aerosols depend on the wind speed at emission? *Atmospheric Chemistry and Physics*, *11*(19), 10149–10156. https://doi.org/10.5194/acp-11-10149-2011

Labiadh, M., Bergametti, G., Kardous, M., Perrier, S., Grand, N., Attoui, B., et al. (2013). Soil erosion by wind over tilled surfaces in South Tunisia. *Geoderma*, *202–203*, 8–17. https://doi.org/10.1016/j.geoderma.2013.03.007

Li, D., & Bou-Zeid, E. (2011). Coherent structures and the dissimilarity of turbulent transport of momentum and scalars in the unstable atmospheric surface layer. *Boundary-Layer Meteorology*, *140*(2), 243–262. https://doi.org/10.1007/s10546-011-9613-5

de Longueville, F., Ozer, P., Doumbia, S., & Henry, S. (2013). Desert dust impacts on human health: an alarming worldwide reality and a need for studies in West Africa. *International Journal of Biometeorology*, *57*(1), 1–19. https://doi.org/10.1007/s00484-012-0541-y

Marticorena, B., & Bergametti, G. (1995). Modeling the atmospheric dust cycle: 1. Design of a soil-derived dust emission scheme. *Journal of Geophysical Research*, *100*(D8), 16415–16430.

Marticorena, B., Kardous, M., Bergametti, G., Callot, Y., Chazette, P., Khatteli, H., et al. (2006). Surface and aerodynamic roughness in arid and semiarid areas and their relation to radar backscatter coefficient. *Journal of Geophysical Research*, *111*, F03017. https://doi.org/10.1029/2006JF000462

Min, Q.-L., Li, R., Lin, B., Joseph, E., Wang, S., Hu, Y., et al. (2009). Evidence of mineral dust altering cloud microphysics and precipitation. *Atmospheric Chemistry and Physics*, *9*(9), 3223–3231. https://doi.org/10.5194/acp-9-3223-2009

Monin, A. S., & Obukhov, A. M. (1954). Basic laws of turbulent mixing in the surface layer of the atmosphere. *Tr. Akad. Nauk SSSR Geophiz. Inst.*, *24*(151), 163–187.

Morman, S. A., & Plumlee, G. S. (2013). The role of airborne mineral dusts in human disease. *Aeolian Research*, *9*, 203–212. https://doi.org/10.1016/j.aeolia.2012.12.001

Nowak, S., Lafon, S., Caquineau, S., Journet, E., & Laurent, B. (2018). Quantitative study of the mineralogical composition of mineral dust aerosols by X-ray diffraction. *Talanta*, *186*, 133–139. https://doi.org/10.1016/j.talanta.2018.03.059

Okin, G. S., Mahowald, N., Chadwick, O. A., & Artaxo, P. (2004). Impact of desert dust on the biogeochemistry of phosphorus in terrestrial ecosystems. *Global Biogeochemical Cycles*, *18*(2), GB2005. https://doi.org/10.1029/2003GB002145

Owen, P. R. (1964). Saltation of uniform grains in air. *Journal of Fluid Mechanics*, *20*(2), 225–242. https://doi.org/10.1017/S0022112064001173

Paulson, C. A. (1970). The mathematical representation of wind speed and temperature profiles in the unstable atmospheric surface layer. *Journal of Applied Meteorology*, *9*(6), 857–861. https://doi.org/10.1175/1520-0450(1970)009<0857:TMROWS>2.0.CO;2

Porch, W. M., & Gillette, D. A. (1977). A comparison of aerosol and momentum mixing in dust storms using fast-response instruments. *Journal of Applied Meteorology*, *16*, 1273–1281.

Prospero, J. M. (1999). Long-range transport of mineral dust in the global atmosphere: Impact of African dust on the environment of the southeastern United States. *Proceedings of the National Academy of Sciences*, *96*(7), 3396–3403.

Rajot, J. L., Alfaro, S. C., Gomes, L., & Gaudichet, A. (2003). Soil crusting on sandy soils and its influence on wind erosion. *Catena*, *53*(1), 1–16. https://doi.org/10.1016/S0341-8162(02)00201-1

Raupach, M. R. (1991). Saltation layers, vegetation canopies and roughness lengths. *Acta Mechanica*, *Suppl 1*, 83–96. https://doi.org/10.1007/978-3-7091-6706-9_5

Redelsperger, J.-L., Thorncroft, C. D., Diedhiou, A., Lebel, T., Parker, D. J., & Polcher, J. (2006). African Monsoon Multidisciplinary Analysis: An international research project and field campaign. *Bulletin of the American Meteorological Society*, *87*(12), 1739–1746. https://doi.org/10.1175/BAMS-87-12-1739

Richardson, L. F. (1920). The supply of energy from and to atmospheric eddies. *Proceedings of the Royal Society A - Mathematical, Physical and Engineering Sciences*, *97*(686), 354–373. https://doi.org/10.1098/rspa.1920.0039

Sassen, K., DeMott, P. J., Prospero, J. M., & Poellot, M. R. (2003). Saharan dust storms and indirect aerosol effects on clouds: CRYSTAL-FACE results. *Geophysical Research Letters*, *30*(12), 1633. https://doi.org/10.1029/2003GL017371

Schütz, L. (1980). Long range transport of desert dust with special emphasis on the Sahara. *Annals of the New York Academy of Sciences*, *338*(1), 515–532.

Shao, Y. (2001). A model for mineral dust emission. *Journal of Geophysical Research*, *106*(D17), 20239–20254.

Shao, Y. (2008). *Physics and modelling of wind erosion* (2nd revised and expanded edition). Heidelberg, Germany: Springer.

Shao, Y., & Li, A. (1999). Numerical modelling of saltation in the atmospheric surface layer. *Boundary-Layer Meteorology*, *91*(2), 199–225.

Shao, Y., Raupach, M. R., & Findlater, P. A. (1993). Effect of saltation bombardment on the entrainment of dust by wind. *Journal of Geophysical Research*, *98*(D7), 12719–12726.

Shao, Y., Ishizuka, M., Mikami, M., & Leys, J. F. (2011). Parameterization of size-resolved dust emission and validation with measurements. *Journal of Geophysical Research*, *116*, D08203. https://doi.org/10.1029/2010JD014527

Smedman, A.-S., Högström, U., Hunt, J. C. R., & Sahlée, E. (2007). Heat/mass transfer in the slightly unstable atmospheric surface layer. *Quarterly Journal of the Royal Meteorological Society*, *133*(622), 37–51. https://doi.org/10.1002/qj.7

Sokolik, I. N., & Toon, O. B. (1996). Direct radiative forcing by anthropogenic airborne mineral aerosols. *Nature*, *381*, 681–683.

Sokolik, I. N., Winker, D. M., Bergametti, G., Gillette, D. A., Carmichael, G., Kaufman, Y. J., et al. (2001). Introduction to special section: Outstanding problems in quantifying the radiative impacts of mineral dust. *Journal of Geophysical Research*, *106*(D16), 18015–18027.

Sow, M., Alfaro, S. C., Rajot, J. L., & Marticorena, B. (2009). Size resolved dust emission fluxes measured in Niger during 3 dust storms of the AMMA experiment. *Atmospheric Chemistry and Physics*, *9*(12), 3881–3891.

Sterk, G., Herrmann, L., & Bationo, A. (1996). Wind-blown nutrient transport and soil productivity changes in southwest Niger. *Land Degradation & Development*, *7*(4), 325–335.

Stull, R. B. (1988). *An introduction to boundary layer meteorology*. Dordrecht, The Netherlands: Kluwer Academic Publishers. https://doi.org/10.1007/978-94-009-3027-8_1

Swap, R., Garstang, M., Greco, S., Talbot, R., & Kållberg, P. (1992). Saharan dust in the Amazon Basin. *Tellus*, *44B*, 133–149.

Vanderpool, R. W., Krug, J. D., Kaushik, S., Gilberry, J., Dart, A., & Witherspoon, C. L. (2018). Size-selective sampling performance of six low-volume “total” suspended particulate (TSP) inlets. *Aerosol Science and Technology*, *52*(1), 98–113. https://doi.org/10.1080/02786826.2017.1386766

Wang, L.-P., & Stock, D. E. (1993). Dispersion of heavy particles by turbulent motion. *Journal of the Atmospheric Sciences*, *50*(13), 1897–1913.

Webb, E. K. (1970). Profile relationships: the log-linear range, and extension to strong stability. *Quarterly Journal of the Royal Meteorological Society*, *96*(407), 67–90. https://doi.org/10.1002/qj.49709640708

Webb, N. P., Chappell, A., Strong, C. L., Marx, S. K., & McTainsh, G. H. (2012). The significance of carbon-enriched dust for global carbon accounting. *Global Change Biology*, *18*(11), 3275–3278. https://doi.org/10.1111/j.1365-2486.2012.02780.x

Weinzierl, B., Ansmann, A., Prospero, J. M., Althausen, D., Benker, N., Chouza, F., et al. (2017). The Saharan Aerosol Long-Range Transport and Aerosol–Cloud-Interaction Experiment: Overview and selected highlights. *Bulletin of the American Meteorological Society*, *98*(7), 1427–1451.

Wieringa, J. (1993). Representative roughness parameters for homogeneous terrain. *Boundary-Layer Meteorology*, *63*(4), 323–363. https://doi.org/10.1007/BF00705357